DOI 10.1007/s11041-024-01073-7
Metal Science and Heat Treatment, Vol. 66, Nos. 7 – 8, November, 2024 (Russian Original Nos. 7 – 8, July – August, 2024)

STEELS FOR GENERAL ENGINEERING PURPOSES

UDC 539.377:669.15-194:539.25:539.42

MORPHOLOGY OF SECONDARY PHASE PARTICLES AND STABILITY OF SUBGRAIN STRUCTURE IN MARTENSITIC STEEL 10Cr9Co3W2MoVNbB (ASTM A335 P92) UNDER CREEP CONDITIONS

E. S. Tkachev[1] and R. O. Kaibyshev[1]

Translated from *Metallovedenie i Termicheskaya Obrabotka Metallov*, No. 8, pp. 22 – 29, August, 2024.

Original article submitted February 12, 2024.

The creep behavior of high-chromium martensitic steel 10Cr9Co3W2MoVNbB (ASTM A335 P92) at a temperature of 650°C and stresses 100 – 180 MPa is studied. The effect of creep on the subgrain structure and the characteristics of secondary particles are determined using transmission electron microscopy. Thermodynamic calculations are performed to determine the volume fraction of precipitates after heat treatment and creep. Precipitation of $(Fe, Cr)_2(W, Mo)$ Laves phase particles and of $(Fe, Cr)_{23}(C, B)_6$ and (Nb, V)(C, N) particles is observed after short-term creep for 243 h. It is shown that pronounced coarsening of the Laves phase particles leads to a decrease in dispersion strengthening under conditions of long-term creep. Creep is accompanied by a decrease in dislocation density and an increase in the subgrain size. It is concluded that the change in the creep power-law exponent upon transition to long-term tests at 650°C is associated with degradation of microstructure, namely, with a pronounced increase in the subgrain size due to a decrease in the density of secondary particles which inhibit the migration of subgrain boundaries.

Key words: high-chromium martensitic steel, creep, subgrain structure, coarsening of precipitates.

INTRODUCTION

Heat-resistant steel 10Kh9K3V2MFBR (10Cr9Co3W2MoVNbB) has been designed as a structural material for high-temperature components of new-generation power equipment operating at super-supercritical steam parameters [1, 2]. The chemical composition and the heat treatment of steel 10Kh9K3V2MFBR are close to those of steel ASTM A335 P92 that has proved its suitability in foreign countries when used in steam conduits of power units due to its refractoriness, relatively low cost, and high creep resistance at up to 620°C [3, 4]. The low critical cooling rate of high-chromium refractory steels makes it possible to form a high-fineness structure of lath martensite by austenitization and subsequent air cooling. The temperature range of 700 – 800°C is typical for tempering of these steels. The tempering reduces the quenching stresses due to redistribution of dislocations and precipitation of carbide particles from the supersaturated solid solution accompanied by formation of a subgrain structure with enhanced stability and precipitation hardening [5]. The heat treatment of steel 10Kh9K3V2MFBR yields secondary particles of two principal types in the structure, i.e., $M_{23}(C, B)_6$ carbides (M is used for Cr and Fe atoms) and MX carbonitrides (M is used for Nb, and V atoms and X is used for C and N atoms) [6].

Prediction of the deformation behavior of heat-resistant steels based on the laws of evolution of their microstructure is an important task, because the determination of the creep characteristics in long-term tests takes much time and resources. It is assumed that the refractoriness of martensitic steels is a result of the high density of intercrystalline boundaries inherited from the structure of lath martensite after tempering [5 – 7]. Development of recrystallization processes in such a structure is extremely undesirable because it causes little predictable early fracture [8]. This explains why the attention in the development of advanced high-chromium

[1] Belgorod State National Research University, Belgorod, Russia (e-mail: tkachev_e@bsu.edu.ru).

steels is mostly devoted to raising the fineness and stability of the particles of second phases, which are located on the boundaries, reduce the interphase energy, and hinder the migration and merging of the boundaries at elevated temperatures [9, 10]. Determination of the interrelation between the evolution of the microstructure and the variation of the creep resistance in operation is very important for improvement of the alloying scheme and development of novel methods of heat and thermomechanical treatments of the alloys.

The aim of the present work was to study the effect of the evolution of the subgrain structure and of the characteristics of the particles of secondary phases on the creep resistance of steel 10Kh9K3V2MFBR at 650°C.

METHODS OF STUDY

We studied high-chromium martensitic steel of the following chemical composition (in wt.%): 0.10 C, 9.05 Cr, 2.80 Co, 1.56 W, 0.58 Mo, 0.41 Mn, 0.20 V, 0.05 Nb, 0.12 Si, 0.012 B, 0.007 N, the remainder Fe.

The steel melted by the vacuum induction method was subjected to 12-h homogenizing annealing at 1150°C, forging at this temperature, and air cooling. The final heat treatment of the steel before testing for creep resistance consisted in austenitization at 1060°C for 30-min, air quenching, and subsequent tempering at 750°C for 3 h.

The creep tests were conducted at 650°C for flat samples with functional part 25 mm long and cross section 7.0 × 3.0 mm using ATS2330 lever testing machines at applied stresses 180, 160, 140, 118 and 100 MPa.

The fine structure of the steel and the second phase particles were studied using a JEOL JEM-2100 transmission electron microscope (TEM) at an accelerating voltage of 200 kV. The second phases were identified by analyzing their chemical composition with the help of an incorporated INCA energy dispersive x-ray analyzer.

After the creep tests, we cut plates with a thickness of 0.3 mm from the samples in the region of uniform elongation to study the microstructure. The plates were thinned in a grinding machine to a thickness of 150 μm. The thin plates were used to knock out discs with diameter 3 mm. The thin foils for TEM were prepared from the discs using jet electropolishing in a 10% solution of $HClO_4$ in CH_3COOH at a voltage of 21 V. To obtain carbon extraction replicas, the polished surface of the functional part of the specimen was etched in an aqueous solution containing 2% nitric acid and 1% hydrofluoric acid. After the etching, the surface of the specimens was covered with a carbon film using a Jeol JEE-200 vacuum machine. Then the carbon films with the particles were put onto copper grids with diameter 3 mm for the TEM study. The size of the subgrains was determined by the random linear intercept method. The dislocation density was determined by calculating individual dislocations on the surfaces of the thin foils under the conditions of multiple diffraction contrast [11].

The precipitates of particles of secondary phases for the x-ray diffraction analysis (XRD) were obtained by dissolving the functional part of the specimen in a 5% solution of HCl in C_2H_5OH at a voltage of 20 V. Then the precipitates were washed in distilled water, centrifuged, and dried at room temperature. The x-ray diffraction analysis of the precipitates was made using a Rigaku Ultima IV diffractometer in copper K_α radiation at scanning angles $2\theta = 35 – 110°$.

The equilibrium volume fraction of the second phase particles was determined by thermodynamic computations using the Termo-Calc software with TCFE7 database for steels.

RESULTS AND DISCUSSION

Creep characteristics of steel 10Kh9K3V2MFBR at 650°C. The dependences of the strain (ε) on the creep time (t) and of the minimum creep rate ($\dot{\varepsilon}_{min}$) on the applied stress (σ) at 650°C are presented in Fig. 1. When the applied stress is decreased from 180 to 100 MPa, the time to failure of the samples increases by about two orders of magnitude from 243 to 17,863 h (Fig. 1*a*). The power dependence of the creep rate on the applied stress exhibits an obvious inflection at σ = 140 MPa (Fig. 1*b*). Therefore, we may distinguish two regions, i.e., a short-term creep lasting for $t < 5000$ h and a long-term creep at $t > 5000$ h.

The variation of the creep exponent (n) may be associated both with the variation of the mechanisms controlling the deformation and with the development of the softening processes due to degradation of the microstructure under the action of the stresses at the elevated temperature. The relatively high value $n = 10 – 17$ indicates marked decrease in the creep rate with lowering of the stress. A similar effect has been observed earlier in precipitation-hardened heat-technology steels under the conditions of short-term creep [12, 13]. Such deformation behavior has been associated with the relatively high density of dislocations, the motion of which is hindered by the second phase particles, carbides $M_{23}C_6$ and carbonitrides MX in the first turn [14, 15]. It should be noted that the formation of particles of an intermetallic Laves phase $(Fe, Cr)_2(W, Mo)$ in short-term creep has been understood as a negative factor due to the decrease in the degree of solid-solution hardening with W and Mo [3]. However, it has been shown in recent works that the precipitation hardening due to the particles of this phase arising in the transition creep stage raises the creep resistance, whereas the coarsening of the particles in long-term test causes softening of the steel [10, 12, 14]. The experimentally observed exponent $n = 6$ in the steel studied under the conditions of long-term tests corresponds to the range of the development of creep ($n = 4 – 7$) controlled by the dislocation climb. The creep rate under such conditions depends substantially on the density of the second phase particles retarding the dislocation slip and hindering the migration of subgrain boundaries.

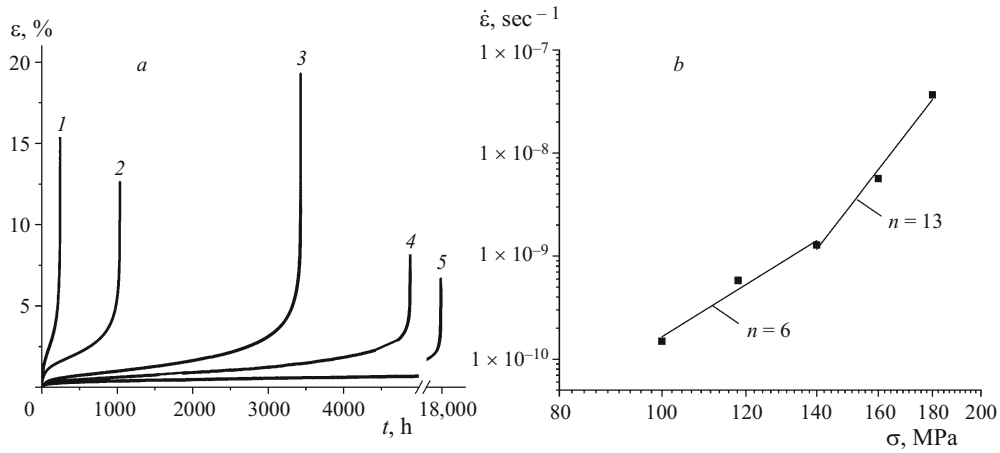

Fig. 1. Creep curves $\varepsilon(t)$ (*a*) and dependence of the minimum creep rate on the applied stress $\dot{\varepsilon}_{min}$ (*b*) for steel 10Kh9K3V2MFBR at 650°C: *1*) σ = 180 MPa, t = 243 h; *2*) σ = 160 MPa, t = 1035 h; *3*) σ = 140 MPa, t = 3430 h; *4*) σ = 118 MPa, t = 4883 h; *5*) σ = 100 MPa, t = 17,863 h.

Effect of creep on the phase composition and subgrain structure of steel 10Kh9K3V2MFBR. The structure of the steel after 30-min quenching from 1060°C in air and 3-h tempering at 750°C is presented in Fig. 2. The boundaries of the initial austenite grains after the etching are well observable under the optical microscope; their average size is 26 μm (Fig. 2*a*). The study of the thin foil in this condition has shown the presence of a great number of particles arranged primarily over the boundaries of martensite laths (Fig. 2*b*). The equilibrium volume fractions of the particles at the temperatures of the tempering (750°C) and of the creep (650°C) computed in Thermo-Calc are presented in Table 1. The predicted phase composition agrees well with the experimental data indicating that the structure of the steel tempered at 750°C contains only particles of $M_{23}C$, $B)_6$ and (Nb, V)(C, N) [16]. After the tests at 650°C, the equilibrium volume fraction of the $(Fe, Cr)_2(W, Mo)$ particles amounts to about 1%. The volume fractions of $M_{23}(C, B)_6$ and (Nb, V)(C, N) remain virtually invariable when the temperature is lowered from 750 to 650°C.

Figure 3 presents the results of the XRD of precipitates after 17,863-h creep. The creep at 650°C is accompanied by precipitation of $(Fe, Cr)_2(W, Mo)$ intermetallic particles. The TEM study of carbon replicas from the surface of the steel has shown that the particles of $(Fe, Cr)_2(W, Mo)$ exceed considerably the particles of $M_{23}(C, B)_6$ and (Nb, V)(C, N) in the size and in the coarsening rate both under the short-term and long-term creep (Table 1). The size of the Laves phase particles attains about 1 μm in 17863 h of the creep test (Fig. 4*a*). The (Nb, V)(C, N) carbonitrides exhibit the lowest susceptibility to coarsening in 17863 h, and their average size grows by less than 50% (from 35 to 52 nm).

The plastic deformation under creep causes growth of subgrains and lowers the dislocation density (Table 1). The

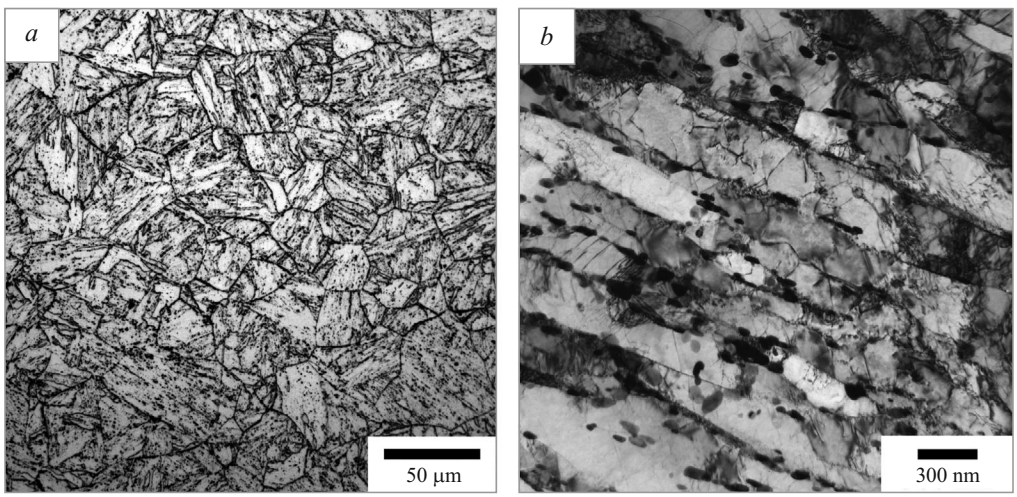

Fig. 2. Structure of steel 10Kh9K3V2MFBR after heat treatment: *a*) optical microscope; *b*) TEM.

relatively equiaxed subgrains with an average size $\overline{\lambda} = 565$ nm form in 243 h at the applied voltage of 180 MPa (Fig. 5). Thus, the average size of subgrains after the short-term creep exceeds the average width of the laths in the steel after the heat treatment. We may conclude that the formation of equiaxed subgrains occurs during the creep jointly with broadening of the laths, i.e., is accompanied by migration of the initial low-angle boundaries. The considerable scattering of the subgrain sizes after the long-term creep is explainable by nonuniform distribution of the fine particles located chiefly over the intercrystalline boundaries. The growth of the coarser particles due to dissolution of the smaller ones (Ostwald ripening) results in formation of structure regions virtually free of particles. In this turn, this process promotes migration of subgrain boundaries and formation of coarse subgrains in these regions.

It is known that the subgrains grow with increase in the degree of the deformation until they reach a stationary size λ_{max}, which depends on the applied stress σ in accordance with the equation [17, 18]

$$\lambda_{max} = \frac{10Gb}{\sigma}, \quad (1)$$

where $G = 77.1$ GPa is the shear modulus at 650°C and $b = 0.248$ nm is the Burgers vector.

The density of mobile dislocations ρ_m in the steady stage also depends on the stress applied [18]:

$$\rho_m = (\sigma/0.5MGb)^2, \quad (2)$$

where $M = 3.06$ is the Taylor factor. Figure 6 presents the dependences of the subgrain size and of the dislocation density on the applied stresses obtained experimentally and by computation with the use of Eqs. (1) and (2). The experimental data prove the inverse linear dependence of the subgrain size on the stress applied (Fig. 6*a*). The size of subgrains in the studied steel does not attain a stationary value λ_{max} either in the short-term creep or in the long-term one. However, the more manifested growth of the size of subgrains at low

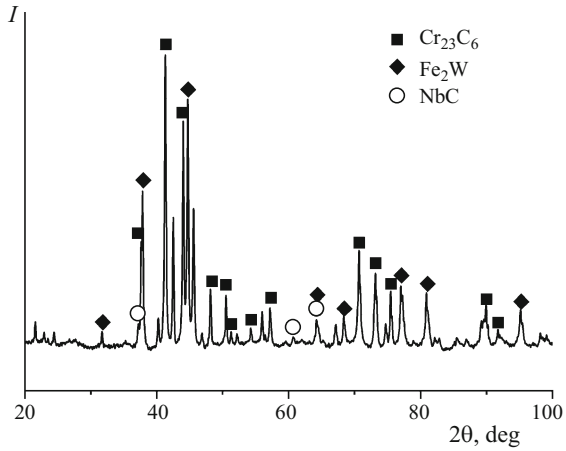

Fig. 3. Results of XRD of second phase particles in steel 10Kh9K3V2MFBR after creep tests for 17,863 h at 650°C.

stresses allows us to think that the growth of subgrains in the steel studied may be the cause of changes in the creep resistance upon transition to longer tests. The relatively high dislocation density $(1.10 \pm 0.35) \times 10^{14}$ m^{-2} is preserved in the steel after the creep at 180 MPa for 243 h (Fig. 6*a*). Increase of the applied stresses from 100 to 160 MPa in the creep tests does not affect substantially the dislocation density inside subgrains. Thus, the dislocation hardening in the structure is about the same in the short-term and long-term creep tests.

The particles of secondary phases hinder the migration of boundaries due to reduction of the interphase energy, and the retarding force (the Zener force P_Z^i) due to each type of the particles can be calculated using the assumption of their uniform distribution and spherical shape with allowance for the volume fraction F_V and for the average particle size d_{av} by the formula [19]

$$P_Z = 3\gamma \frac{F_V}{d_{av}}, \quad (3)$$

where $\gamma = 0.153$ J/m^2 is the specific energy of subgrain boundaries [20].

TABLE 1. Characteristics of Subgrain Structure and Sizes of Second Phase Particles for Different States of the Steel

State	Mode of HT or testing	$\overline{\lambda}$, μm	ρ, × 10^{14} m^{-2}	d_{av}, nm		
				$M_{23}C_6$ carbide	MX carbonitride	Laves phase
Initial (after HT)	Quenching from 1050°C, tempering at 750°C for 3 h	0.30 ± 0.02	2.60 ± 0.50	66	35	—
After creep testing at 650°C	180 MPa, 243 h	0.57 ± 0.04	1.10 ± 0.35	76	35	165
	160 MPa, 1035 h	0.62 ± 0.04	0.45 ± 0.19	86	38	225
	140 MPa, 3430 h	0.78 ± 0.06	0.45 ± 0.19	107	40	283
	118 MPa, 4883 h	0.91 ± 0.05	0.41 ± 0.26	114	40	367
	100 MPa, 17863 h	1.28 ± 0.12	0.38 ± 0.15	142	52	525

Notations: λ) size of subgrains; ρ) density of lattice dislocations; d_{av}) average grain size.

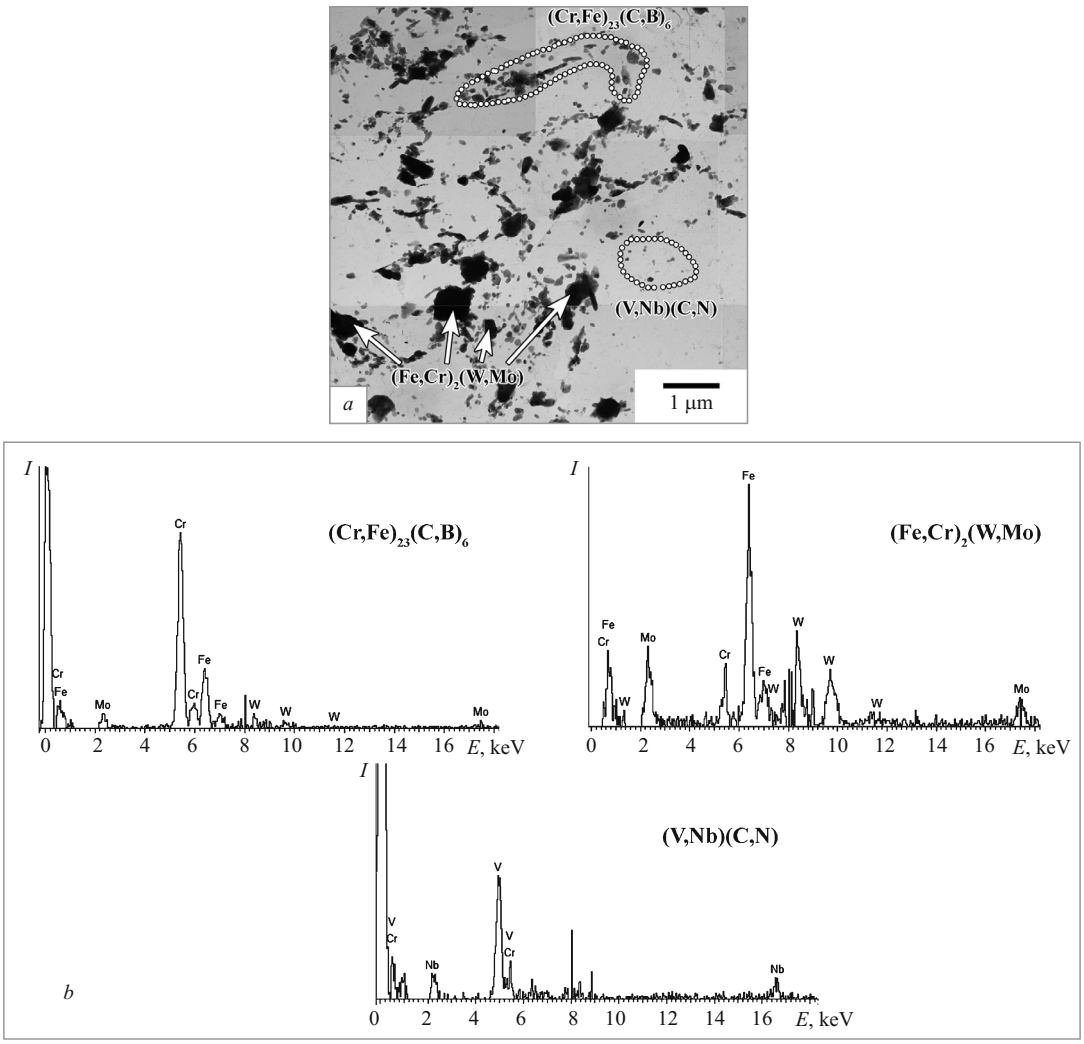

Fig. 4. Second phase particles (*a*) and results of energy dispersive analysis of individual particles (*b*) on a carbon extraction replica taken from a sample of steel 10Kh9K3V2MFBR after creep tests for 17,863 h at 650°C (TEM).

The calculated variation of the retarding forces that stabilize the subgrain structure in the creep process is presented in Fig. 7. It can be seen that for all the states studied the particles of $M_{23}(C, B)_6$ make the highest contribution into the re-

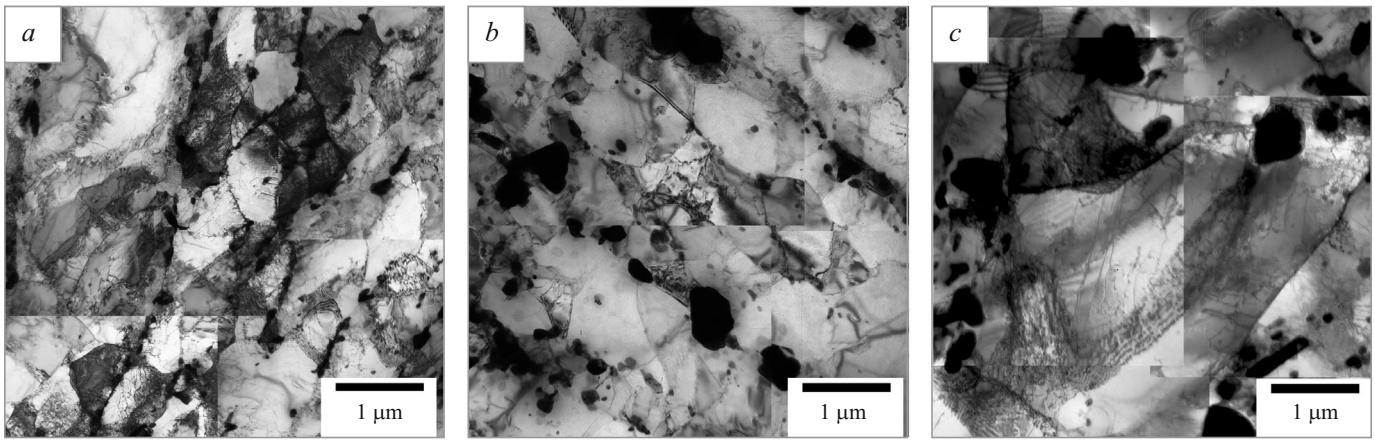

Fig. 5. Evolution of subgrain structure (TEM) in steel 10Kh9K3V2MFBR after creep to failure at different applied stresses: *a*) σ = 180 MPa, average subgrain size $\overline{\lambda}$ = 565 nm; *b*) σ = 140 MPa, $\overline{\lambda}$ = 780 nm; *c*) σ = 100 MPa, $\overline{\lambda}$ = 1280 nm.

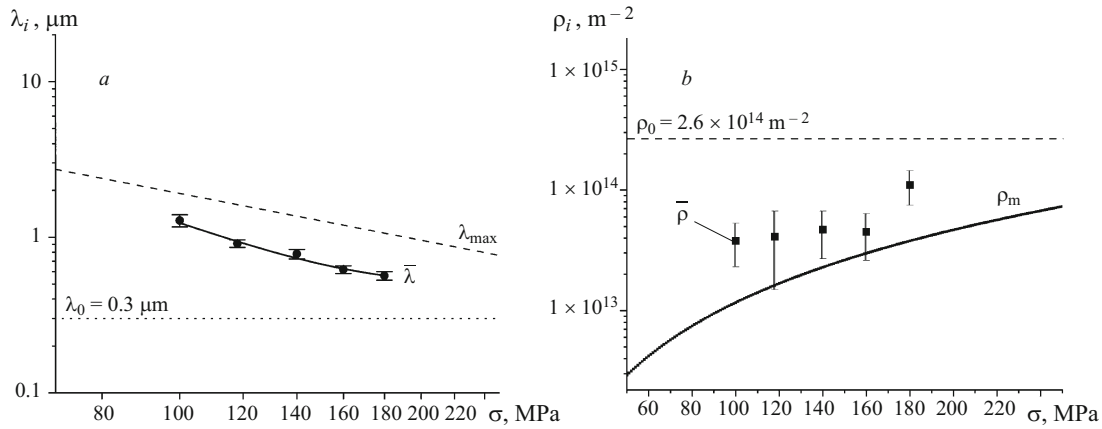

Fig. 6. Dependence of the experimental ($\bar{\lambda}$) and computed (λ_{max}) subgrain sizes (*a*) and of the density of mobile lattice dislocations (ρ_m — computation; $\bar{\rho}$ — experiment) on applied stresses in creep tests of steel 10Kh9K3V2MFBR: λ_0, ρ_0) initial subgrain size and dislocation density, respectively.

tarding forces, which is connected with their higher volume fraction and relatively low size of about 100 nm (Table 1). In short-term creep lasting for up to 1×10^3 h, the summed retarding forces are higher than in the steel after tempering. This is explainable by precipitation of $(Fe, Cr)_2(W, Mo)$ particles in the structure, which more than compensates the decrease in the retarding forces due to the coarsening of carbides and carbonitrides. It should be noted that the earlier experimental data show that the content of tungsten in the solid solution of the steel decreases from 0.96 to 0.32 at.% in 1×10^3 h of annealing/creep at 650°C and then changes insubstantially [10]. This means that the process of precipitation/growth of particles from the supersaturated solid solution has stopped giving way to the stage of their Ostwald ripening at this temperature. When the time before failure increases from 243 to 17863 h, the summed retarding force is halved (from 0.20 to 0.10 MPa). In work [21] devoted to the relation between the creep resistance and the microstructure of a steel with composition P92 + 3% Co the critical value of the retarding forces at which the subgrains start to grow intensely amounts to about 0.12 MPa. The time before failure at a stress of 140 MPa corresponding to the inflection point on the curve of the long-tern strength is about twice higher in the steel studied than in steel P92 + 3% Co. This difference seems to be explainable by the elevated content of boron in the steel studied, which provides a smaller size and a lower rate of coarsening of the particles of $M_{23}(C, B)_6$ [22]. The nanosize carbonitrides of type MX are characterized by a very low coarsening rate, but their influence on the stability of subgrain boundaries is not significant due to their low volume fraction.

It should be noted that the distribution of different types of particles in the structure differs substantially. The particles of $(Fe, Cr)_2(W, Mo)$ and $M_{23}(C, B)_6$ are chiefly located on the intercrystalline boundaries, whereas the larger part of the MX carbonitrides resides inside the martensite laths. The particles of the $M_{23}(C, B)_6$ carbonitride and of the Laves phase make a great contribution into stabilization of subgrain boundaries and hinder the process of knitting-out of dislocations from the low-angle lath boundaries. The uniformly distributed MX carbonitrides hinder the motion of dislocations inside the laths [23]. Therefore, the evolution of the precipi-

TABLE 2. Equilibrium Content of Second Phase Particles in Steel 10Kh9K3V2MFBR in Different States

State	Equilibrium fraction of particles (vol.%)		
	$M_{23}C_6$ carbide	Laves phase	MX carbonitrides
After tempering at 750°C	2.112	0	0.090
After creep testing at 650°C	2.159	0.962	0.086

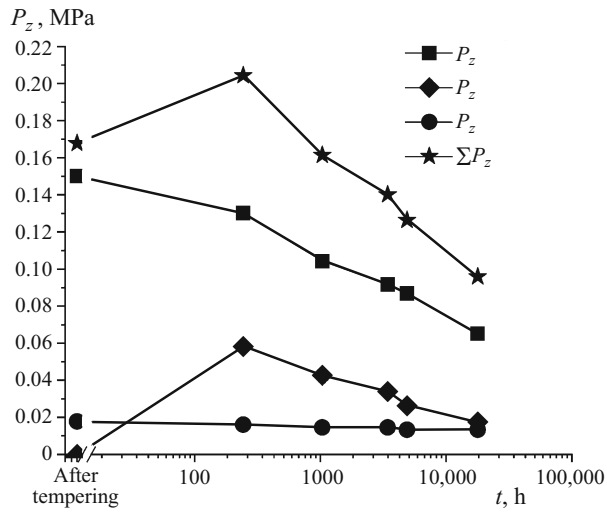

Fig. 7. Retarding forces P_z acting on subgrain boundaries as a function of the duration of creep tests of steel 10Kh9K3V2MFBR.

tation hardening with particles of different types should be considered with allowance for the parameters of the particles arranged on boundaries of different types and awaits further study.

The results obtained show that the variation of the creep exponent of steel 10Kh9K3V2MFBR upon transition to long tests at 650°C correlates with the increase in the growth rate of subgrains. The main factor responsible for degradation of the microstructure of the steel is the coarsening of the grain boundary particles of $(Fe, Cr)_2(W, Mo)$ and $M_{23}(C, B)_6$.

CONCLUSIONS

The results of the study of the effect of the evolution of subgrain structure and of the characteristics of the particles of secondary phases on the creep resistance of steel 10Kh9K3V2MFBR at 650°C allow us to make the following conclusions.

1. Martensitic steel 10Kh9K3V2MFBR possesses a very high creep resistance in the range of high stresses ($\sigma^{650°C}_{1000\ h} = 140$ MPa, $\dot{\varepsilon}_{min} = 1.28 \times 10^{-9}\ sec^{-1}$), but its refractoriness tends to lower in long-term tests at 650°C. When the applied stresses are reduced from 180 – 140 to 140 – 100 MPa, the creep exponent *n* falls from 13 to 6.

2. The plastic deformation under the creep causes lowering of the dislocation density and growth of subgrains in the structure of the steel. The density of the lattice dislocations after the creep at a stress below 160 MPa amounts to about $0.4 \times 10^{14}\ m^{-2}$. Under the conditions of long-term creep, the size of the subgrains tends to attain a stationary value with decrease of the applied stresses, which correlates with the slope of the curves describing the dependence $\dot{\varepsilon}_{min} - \sigma$.

3. The stability of the subgrain structure of the steel in short-term creep increases due to the additional contribution of the retarding forces produced by the nucleating particles of the $(Fe, Cr)_2(W, Mo)$ intermetallic phase. This compensates the coarsening of the carbide and carbonitride particles and provides a high high-temperature strength. Intense coarsening of the particles of $(Fe, Cr)_2(W, Mo)$ starts after 1×10^3 h of creep at 650°C.

4. The main reason behind the lowering of the stability of subgrain boundaries under long-term creep is coarsening of the grain boundary particles of $(Fe, Cr)_2(W, Mo)$ and $M_{23}(C, B)_6$. The MX carbonitrides are little susceptible to coarsening, but influence little the migration of the boundaries due their relatively low volume fraction.

DECLARATIONS

Funding

This study gas been supported financially by the Russian Science Foundation, grant No. 23-79-01178 (https://rscf.ru/project/23-79-01178/). The author thanks the Joint Research Center "Technology and Materials" of the Belgorod State National Research University.

Credit Authorship Contribution Statement

E. Tkachev: project administration, conceptualization, methodology, investigation, writing of original draft; *R. Kaibyshev*: conceptualization.

Declaration of Competing Interest

The authors confirm that they have no known financial or interpersonal conflicts that would have appeared to have an impact on the research presented. We are approving the final version of the manuscript.

Availability of Data and Material

Not applicable.

Code Availability

Not applicable.

Supplementary Information

Not applicable.

REFERENCES

1. V. I. Skorobogatykh, I. A. Shchenkova, P. A. Kozlov, et al., "New refractory steels for units with supercritical steam parameters," *Tyazh. Mash*., No. 3, 7 – 10 (2011).
2. S. I. Feklistov, P. A. Kozlov, V. A. Dub, et al., "Development of production process for new-generation high-temperature components of power equipment (SSKP) from nanostructured refractory steels," *Tyazh. Mash*., No. 1, 13 – 18 (2011).
3. P. J. Ennis, A. Zielinska-Lipiec, O. Wachter, et al., "Microstructural stability and creep rupture strength of the martensitic steel P92 for advanced power plant," *Acta Mater.*, **45**(12), 4901 – 4907 (1997).
4. J. Hald and L. Korcakova, "Precipitate stability in creep resistant ferritic steels — experimental investigations and modelling," *ISIJ Int*., **43**(3), 420 – 427 (2003).
5. K. A. Lanskaya, *High-Chromium Heat Resistant Steels* [in Russian], Metallurgiya, Moscow (1976), 216 p.
6. R. O. Kaibyshev, V. N. Skorobogatykh, and I. A. Shchenkova, "Novel steels of martensitic class for power engineering," *Fiz. Met. Matalloved*., **109**(2), 200 – 215 (2010).
7. V. V. Sagaradze, T. N. Kochetkova, N. V. Kataeva, et al., "Structure and creep of Russian reactor steels with BCC-Lattice," *Fiz. Met. Metalloved*., **118**(5), 522 – 534 (2017).
8. A. E. Fedoseeva, "Creep resistance and structure of 10% Cr – 3% Co – 2% W – 0.29% Cu – 0.17% Re steel with low nitrogen content and high content of boron for fabricating components of power units of coal-fired power plants," *Fiz. Mezomekh*., **26**(5), 115 – 130 (2023).
9. V. K. Pal, L. P. Singh, and M. Tarik, "A study of microstructure and mechanical properties of steel P92 after different heat treatments," *Metalloved. Term. Obrab. Met*., No. 3, 13 – 17 (2022).
10. E. Tkachev, A. Belyakov, and R. Kaibyshev, "Creep strength breakdown and microstructure in a 9 % Cr steel with high B and low N contents," *Mater. Sci. Eng. A*, **772**, 138821 (2020).

11. A. P. Zhilyaev, I. Shakhova, A. Morozova, et al., "Grain refinement kinetics and strengthening mechanisms in Cu – 0.3Cr – 0.5Zr alloy subjected to intense plastic deformation," *Mater. Sci. Eng. A*, **654**, 131 – 142 (2016).
12. A. Fedoseeva, E. Tkachev, and R. Kaibyshev, "Advanced heat-resistant martensitic steels: Long-term creep deformation and fracture mechanisms," *Mater. Sci. Eng. A*, **862**, 144438 (2023).
13. M. Yu. Belomytsev, "Experimental analysis of creep laws in heat-resistant ferritic-martensitic steel," *Deform. Razrush. Mater.*, No. 10, 31 – 41 (2019).
14. E. Tkachev, A. Belyakov, and R. Kaibyshev, "Creep behavior and microstructural evolution of a 9% Cr steel with high B and low N contents," *Mater. Sci. Eng. A*, **725**, 228 – 241 (2018).
15. K. V. Almaeva, N. A. Polekhina, and I. Y. Litovchenko, "A comparative investigation of mechanical properties of the ferritic-martensitic steel EK-181 in the temperature range 700 – 800°C after high-temperature thermomechanical and traditional heat treatments," *AIP Conf. Proc*., **2051**(1), Art. 020009 (2018).
16. I. Fedorova, A. Kostka, E. Tkachev, et al., "Tempering behavior of a low nitrogen boron-added 9% Cr steel," *Mater. Sci. Eng. A*, **662**, 443 – 455 (2016).
17. K. Sawada, M. Takeda, K. Maruyama, et al., *Materials Advanced Power Engineering*, Forchungszentrum Julich GmbH, Julich (1998), 575 p.
18. K. Maruyama, K. Sawada, and J. Koike, "Strengthening mechanisms of creep resistant tempered martensitic steel," *ISIJ Int*., **41**(6), 641 – 653 (2001).
19. M. Pa, M. Ferry, and T. Chandra, "Five decades of the Zener equation," *ISIJ Int*., **38**(9), 913 – 924 (1998).
20. A. Fedoseeva, N. Dudova, R. Kaibyshev, et al., "Effect of tungsten on creep behavior of 9% Cr – 3% Co martensitic steels," *Metals*, **7**(12), 573 (2017).
21. A. Fedoseeva, N. Dudova, and R. Kaibyshev, "Creep strength breakdown and microstructure evolution in a 3% Co modified P92 steel," *Mater. Sci. Eng. A*, **654**, 1 – 12 (2016).
22. E. S. Tkachev, A. N. Belyakov, and R. O. Kaibyshev, "Role of deformation in coagulation of particles of $M_{23}C_6$ molybdenum carbide in 9% Cr steel," *Fiz. Met. Metalloved*., **121**(8), 884 – 891 (2020).
23. W. Blum and P. Eisenlohr, "Dislocation mechanics of creep," *Mater. Sci. Eng. A*, **510**, 7 – 13 (2009).